Proceedings of the Fifth IASTED International Conference
POWER AND ENERGY SYSTEMS
June 15-17, 2005, Benalmádena, Spain

NEW SYNCHRONIZATION METHOD FOR THREE-PHASE FOUR-WIRE PWM CONVERTERS UNDER UNBALANCE AND HARMONICS IN THE GRID VOLTAGES

Robinson F. de Camargo and Humberto Pinheiro
Power Electronics and Control Research Group – GEPOC
Federal University of Santa Maria - UFSM
ZIP CODE: 97105-900 – Santa Maria, RS – Brazil
e-mail: robinsonfcamargo@hotmail.com.br, humberto@ctlab.ufsm.br

ABSTRACT
This paper proposes a new *open-loop* synchronization method for three-phase four-wire PWM converters connected to the utility grid. It presents a better performance in terms of distortions in the synchronism signals if compared with other *open-loop* methods. In addition, a frequency adaptation algorithm is proposed for applications where large frequency variations are expected, such as in weak grids. Experimental results using a DSP TMS320F2812 are given to demonstrate the good performance of the proposed synchronism method.

KEY WORDS
Three-Phase Three-Four PWM Converters, Normalized Voltage, Positive Sequence, Synchronous Frame.

1. Introduction

Several techniques to synchronize PWM converters to the utility grid have been reported. They can be classified as *closed-loop* [1-5] and *open-loop* [6-13] methods. In *closed-loop* methods the angle of synchronism is obtained through a closed-loop structure, which aimed at locking the estimated value of the phase angle to its actual value. On the other hand, *open-loop* synchronization methods, the synchronism angle or normalized synchronism vector is obtained directly from the grid voltages [6, 7, 9], virtual flux [8, 10, 11] or estimate grid voltages
[12, 13].
Although *closed-loop* methods have low sensitivity to the grid frequency, a trade off between good transient response and good filtering characteristics must always be considered. Moreover, *cycle slips* phenomenon is usually present in PLL *closed-loop* methods. When these methods are used to synchronize PWM converters to grid, this phenomenon can result in large transient currents during the resynchronization [16].
Among the *open-loop* methods, the modified synchronous reference frame (*MSRF*) [6, 7] and the low-pass filter based (*LPF-B*) methods [9] standout for their simplicity. The main attribute of the former is to be independent of the grid frequency. The later and the extend *Kalman* filter (*EKF*) [5] are less sensitive to the grid harmonics. Moreover, the weighted least-square estimation (*WLSE*) [15] rejects the impact of negative-sequence and accommodates frequency variations. However, none of *open-loop* methods reported, so far, have a good performance in terms of the distortion in synchronism under unbalance and harmonics in the grid voltages.
In this sense, this paper proposes a new *open-loop* synchronization method for three-phase four-wire PWM converters connected to the utility grid that provides a good performance in terms of synchronism signals, even in the presence of harmonics and severe unbalance between the grid voltages. Simulation and experimental results demonstrate the good performance of the proposed method using a DSP TMS320F2812 controller.

2. Proposed Synchronization Method

The proposed synchronization method is called normalized positive sequence synchronous frame, NPSF, and it is shown in the Fig. 1 for three-phase four-wire systems. From the measure of the three phase-to-neutral grid voltages, the normalized positive sequence synchronism vector in the fundamental frequency is obtained.

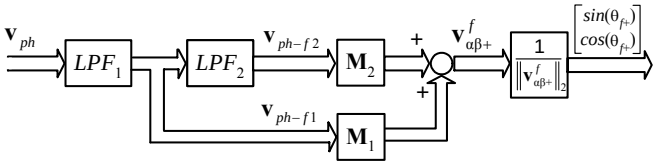

Fig. 1 – Proposed normalized positive sequence reference frame for three-phase four-wire systems.

Let us define a vector where each entry is the fundamental phase-to-neutral voltage is:

$$\mathbf{v}^f_{ph} = \begin{bmatrix} v^f_a \\ v^f_b \\ v^f_c \end{bmatrix}. \qquad (1)$$

Now, by considering that the grid voltages usually have some degree of unbalance, depending on the synchronization method used, this disturbance generates distortion in synchronism signals [2, 19]. As consequence, the currents that are drained by the converters from the grid will also be distorted [14]. To prevent this distortion, the synchronism vector will be generated from the positive sequence components of the grid voltages at the fundamental frequency.

The phase voltage positive sequence at the fundamental frequency can be obtained as follows:

$$\mathbf{v}_{ph+}^{f} = \mathbf{T}_{+seq}\mathbf{v}_{ph}^{f}, \tag{2}$$

where:

$$\mathbf{v}_{ph+}^{f} = \begin{bmatrix} v_{a+}^{f} \\ v_{b+}^{f} \\ v_{c+}^{f} \end{bmatrix}, \mathbf{T}_{+seq} = \begin{bmatrix} 1 & a & a^2 \\ a^2 & 1 & a \\ a & a^2 & 1 \end{bmatrix}, \mathbf{v}_{ph}^{f} = \begin{bmatrix} v_{a}^{f} \\ v_{b}^{f} \\ v_{c}^{f} \end{bmatrix}, \tag{3}$$

$$a = e^{j2\pi/3} = -(1/2) + (\sqrt{3}/2)e^{j\pi/2}, \tag{4}$$

In (3), the superscript *f* and subscript *+seq* represent the fundamental frequency and the positive sequence, respectively. The operator *a* in (4) implements in the time domain the 120º phase-shift originally presented by Fortescue in his theory of symmetrical components applied to phasor quantities. This operator implementation will be addressed in Section 2.1.

A simple way to obtain the synchronism vector is by transforming grid voltages into αβ stationary coordinates [6,7]. In a similar way, here the positive sequence phase voltages at the fundamental frequency will be transformed to αβ coordinates, that is,

$$\mathbf{v}_{\alpha\beta+}^{f} = \mathbf{T}_{\alpha\beta}\mathbf{v}_{ph+}^{f}, \tag{5}$$

where:

$$\mathbf{v}_{\alpha\beta+}^{f} = \begin{bmatrix} v_{\alpha+}^{f} \\ v_{\beta+}^{f} \end{bmatrix}, \mathbf{T}_{\alpha\beta} = \sqrt{\frac{2}{3}}\begin{bmatrix} 1 & -1/2 & -1/2 \\ 0 & \sqrt{3}/2 & -\sqrt{3}/2 \end{bmatrix}, \tag{6}$$

Aiming to simplify the transformations presented in (2) and (5), they can be combined as follows:

$$\mathbf{v}_{\alpha\beta+}^{f} = \mathbf{T}_{\alpha\beta}\mathbf{T}_{+seq}\mathbf{v}_{ph}, \tag{7}$$

which can also be expressed as:

$$\mathbf{v}_{\alpha\beta+}^{f} = \mathbf{M}_1\mathbf{v}_{ph}^{f}e^{-j\pi/2} + \mathbf{M}_2\left(-\mathbf{v}_{ph}^{f}\right), \tag{8}$$

where:

$$\mathbf{M}_1 = \frac{1}{2}\begin{bmatrix} 0 & -\sqrt{2}/2 & \sqrt{2}/2 \\ \sqrt{6}/3 & -\sqrt{6}/6 & -\sqrt{6}/6 \end{bmatrix}, \quad \mathbf{M}_2 = \frac{1}{2}\begin{bmatrix} -\sqrt{6}/3 & \sqrt{6}/6 & \sqrt{6}/6 \\ 0 & -\sqrt{2}/2 & \sqrt{2}/2 \end{bmatrix}. \tag{9}$$

Note that $\mathbf{v}_{\alpha\beta}{}^{f}{}_{+}$ is the grid positive sequence phase voltage vector at the fundamental frequency in αβ coordinates. Thus, its amplitude depends on the grid voltage. A normalized synchronism vector can be obtained dividing $\mathbf{v}_{\alpha\beta}{}^{f}{}_{+}$ by its norm, that is,

$$\mathbf{v}_{\alpha\beta+n}^{f} = \frac{\mathbf{v}_{\alpha\beta+}^{f}}{\left\|\mathbf{v}_{\alpha\beta+}^{f}\right\|_2}, \tag{10}$$

where this Euclidian norm of the vector is given by:

$$\left\|\mathbf{v}_{\alpha\beta+}^{f}\right\|_2 = \sqrt{\left(v_{\alpha+}^{f}\right)^2 + \left(v_{\beta+}^{f}\right)^2}. \tag{11}$$

The entries of the vector $\mathbf{v}_{\alpha\beta}{}^{f}{}_{+n}$ (10) can be understood as being the *sine* and *cosine* often used to synchronize PWM converters with the grid, that is,

$$sin\left(\theta_{f+}\right) = v_{\beta+n}^{f} \text{ and } cos\left(\theta_{f+}\right) = v_{\alpha+n}^{f}, \tag{12}$$

where $\theta_{f+}=\omega_f t$ and ω_f is the grid fundamental frequency.

In order to obtain $\mathbf{v}_{\alpha\beta}{}^{f}{}_{+n}$, it is required to find $\mathbf{v}_{ph}^{f}e^{-j\pi/2}$ e $-\mathbf{v}_{ph}^{f}$. The next section describes how these variables are derived in the time domain.

2.1 Implementation of $e^{-j\pi/2}$ in time domain

In [2], the operator $e^{j\pi/2}$ has been implemented in time domain with all-pass filters, which are designed to provide unit gain and 90º phase-shift at the fundamental frequency. However, this approach does not consider the harmonics in the grid voltages, which corrupts the synchronization signals [2,5].

As an alternative, this paper considers the use of low-pass filters to reduce the harmonics present in $\mathbf{v}_{ph}$ as well as to implement the 90º phase-shift at the fundamental frequency as required to compute the positive sequence.

Therefore, the $\mathbf{v}_{ph}$ vector is firstly filtered using a low-pass filter, LPF_1, which generates a filtered vector, $\mathbf{v}_{l\text{-}l\_f1}$. This vector has its fundamental voltage -90º shifted from the fundamental of $\mathbf{v}_{ph}$ The $\mathbf{v}_{ph\text{-}f1}$ vector is filtered again using another low-pass filter, LPF_2. This provides an additional -90º phase-shift, resulting in the filtered vector $\mathbf{v}_{ph\text{-}f2}$, which presents the same amplitude at the fundamental of the original vector $\mathbf{v}_{l\text{-}l}$, but with -180º phase-shift.

Thereby, the output of the LPF_1 filter will be $\mathbf{v}_{ph}^{f}e^{-j\pi/2}$ and the LPF_2 output will be $-\mathbf{v}_{ph}^{f}$, which are required to compute $\mathbf{v}_{\alpha\beta+}^{f}$.

The low-pass filters LPF_1 and LPF_2 are projected in a similar way. The second order transfer function of the implemented filters in the *s* domain is:

$$G(s) = \frac{\omega_n^2}{s^2 + 2\zeta\omega_n s + \omega_n^2}, \tag{13}$$

Note that the parameters of the filter must be selected so that:

$$G(s)\big|_{s=j\omega_f} = 1\angle -90°, \tag{14}$$

where, *f*=60 Hz. To satisfy this condition, $\omega_n = 2\pi f$ and ζ=0.5.

In the discrete domain, the low-pass filters may be implemented by the following discrete state space equation:

$$\begin{aligned} x(k+1) &= \mathbf{G}x(k) + \mathbf{H}u(k) \\ y(k) &= \mathbf{C}x(k) \end{aligned}, \tag{15}$$

The equation (15) has been obtained by the discretization of (13), using a zero order hold (ZOH) with a sampling period T_s. The frequency response of the *LPF* filter implemented with (15) is shown in Fig. 2. It is possible to see that at 60 Hz, the filter presents a unit gain and a -90º phase-shift. In addition, voltage harmonics are significantly reduced for instance at the output of LPF_1 the 3 rd is attenuated -19 dB and the 5 th, -28 dB. At the

output of LPF_2 the 3 rd is attenuated -38 dB and the 5 th, -56 dB.

Note that the -90º phase-shift occurs at 60Hz. In cases where the grid frequency varies significantly, the filter parameters must be updated. Next Section proposes an adaptation algorithm for the filter parameters.

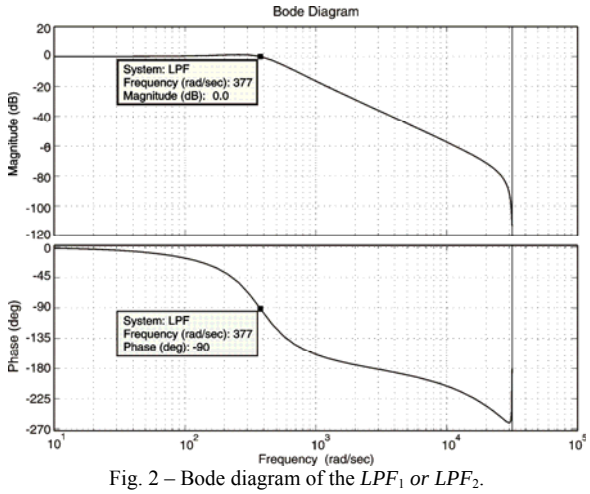

Fig. 2 – Bode diagram of the LPF_1 *or* LPF_2.

3. Frequency Adaption Algorithm

In stiff grids, the frequency variations in the considered algorithm is not a concern, since the utility companies usually provide a grid voltage with frequency regulated between ± 1 Hz, as recommended by IEC 61000-2-2.

However, in isolated energy systems, the frequency variations can exceed the limits mentioned above. So, to broaden the range of applications of the synchronization method to this grid conditions, a frequency adaptation algorithm is proposed. Its block diagram is shown in Fig. 3.

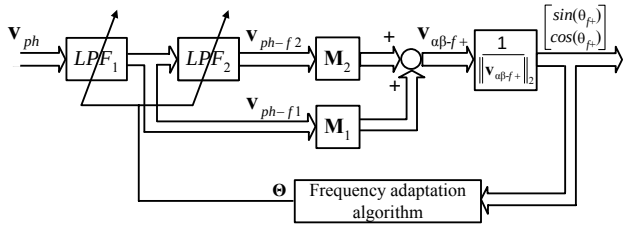

Fig. 3 – Proposed normalized positive sequence reference frame for three-phase four-wire systems with frequency adaptation algorithm.

Details of the frequency adaptation algorithm are given in Fig. 4. It consists of a low-pass filter, LPF_3, identical to LPF_1 and LPF_2. The LPF_3 filters the normalized synchronization vector obtained, (10), and from the result is calculated its square norm, that is,

$$\left\| \mathbf{v}_{sc-f} \right\|_2^2, \tag{16}$$

If the natural frequency of the filter ω_n is equal to the grid frequency, then (16) results in 1. However, if $\|\mathbf{v}_{sc-f}\|_2^2>1$ it indicates that the natural frequency of the filter ω_n is bigger than the grid frequency. On the other hand, if $\|\mathbf{v}_{sc-f}\|_2^2<1$, it indicates that ω_n is smaller than the fundamental frequency of the grid. Then, the error, $1-\|\mathbf{v}_{sc-f}\|_2^2$ can be used to estimate the grid frequency $\hat{\omega}$, using an integrator, as shown in Fig. 4. Then using the $\hat{\omega}$, the matrices **G**, **H** and **C** of the low-pass filters can be updated.

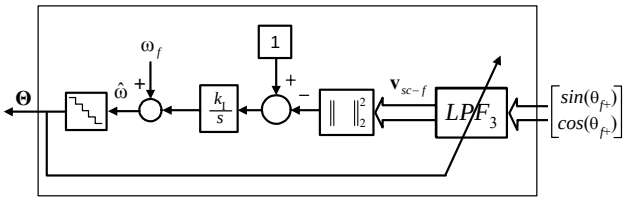

Fig. 4 – Proposed frequency adaptation algorithm.

3.1 Implementation of $e^{-j\pi/2}$ in time domain

Aiming to design the gain of the frequency adaptation algorithm, a nonlinear model will be developed. The block diagram of the nonlinear model of this adaptation algorithm is shown in Fig. 5, where the dynamics of LPF_3 have not been considered. In sinusoidal steady-state, the relationship between $\|\mathbf{v}_{sc-f}\|_2^2$, the grid frequency and the estimated frequency can be expressed as follows:

$$f(\hat{\omega},\omega) = \left\| \mathbf{v}_{sc-f} \right\|_2^2 = \frac{1}{\left[1-\left(\frac{\omega}{\hat{\omega}}\right)^2\right]^2 + \left(\frac{\omega}{\hat{\omega}}\right)^2} \tag{17}$$

By linearizing the system shown in Fig. 5 around the nominal operation point, a linear model is obtained as shown in Fig. 6. This model will be used in the design of the integrator gain.

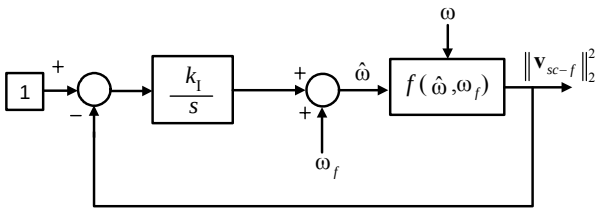

Fig. 5 – Block diagram of the nonlinear model.

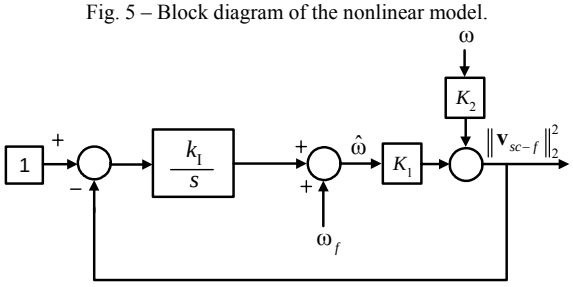

Fig. 6 – Block diagram of the linearized model.

The gains K_1 and K_2 are:

$$K_1 = \left.\frac{\partial f}{\partial \hat{\omega}}\right|_{\hat{\omega}=\omega_f,\omega=\omega_f}, \tag{18}$$

$$K_2 = \left.\frac{\partial f}{\partial \omega}\right|_{\hat{\omega}=\omega_f,\omega=\omega_f}. \tag{19}$$

Thus, substituting (17) in (18) and (19) the gains K_1 and K_2 are obtained, which are:

$$K_1 = -K_2 = \frac{2}{\omega_f}. \quad (20)$$

Finally, by defining the bandwidth of frequency adaptation algorithm as B_ω, the integrator gain can be obtained as follows:

$$k_1 = \frac{B_\omega}{K_1} = \frac{B_\omega \omega_f}{2}. \quad (21)$$

where, ω_f is the grid nominal frequency.

As an example, if the bandwidth of the adaptation algorithm is equal to the grid frequency, that is, $B_\omega = \omega_f / 10$, then $k_1 \cong 14.213$.

Therefore, the frequency estimation algorithm can be summarized as:

$$\hat{\omega} = \omega_f + \frac{k_I}{s}\left(1 - \left\|\mathbf{v}_{sc-f}\right\|_2^2\right). \quad (22)$$

In case there is grid frequency variation, the low-pass filters parameters are updated. In Fig. 4, the parameter $\boldsymbol{\Theta}$ represents the union of the filter matrices, that is, $\boldsymbol{\Theta} = \mathbf{G} \cup \mathbf{H} \cup \mathbf{C}$.

The proposed algorithm transient behavior due to frequency variations is presented in the experimental results section.

4. Performance of the Proposed Method

In this section, the performance of the proposed method in terms of synchronism signals is demonstrated. The *THD* and unbalance factor criteria are used to quantify the grid voltages conditions.

Fig.7. shows the phase-to-neutral grid voltages under harmonics and several unbalanced. In this case, a 5% harmonic distortion in the utility voltages is considered, due to the fact that, typically this value is less than 5%. The 5th, 7 th and 11 th harmonics have been considered in the grid voltages with the same amplitude. Moreover, a severe unbalanced of 25 % in the grid voltages has been added to emphasize the performance of the proposed method.

Fig. 8 presents the *sine* and *cosine* functions used in the *NPSF* method. It is not possible to see significant distortions in the *sine* and *cosine* even under severe unbalanced and harmonics in the grid voltages.

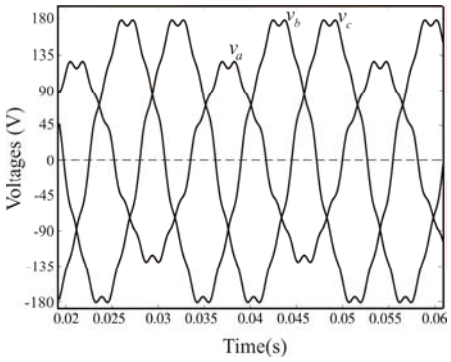

Fig. 7 – Phase-to-neutral grid voltages under THD_v=5 % and Unb_v=25%.

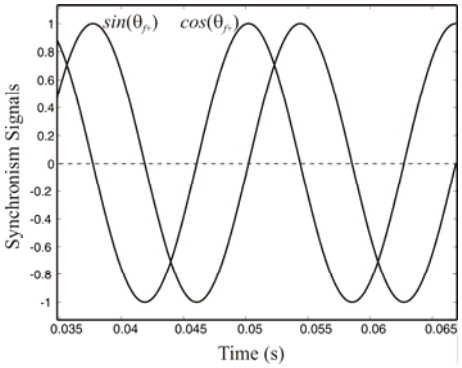

Fig. 8 – *Sine* and *cosine* generate used the *NPSF* method under THD_v=5 % and Unb_v=25 % grid voltages.

Next section presents experimental results of the new synchronism method and the proposed frequency adaptation algorithm.

5. Experimental Results

The proposed synchronization method has been implemented in a TMS320F2812 DSP controller with fixed-point arithmetic. The execution time of the synchronization algorithm took 6.5 μs of the CPU time, allowing rising up the sampling frequency to 40 kHz.

Fig. 9 shows the experimental results of the v_a and v_b phase-to-neutral grid voltages in p.u. under THD_v=0% and Unb_v=0%. Fig. 10 presents the *sine* and *cosine* generated for the *NPSF* method under this condition. Fig. 11 shows the experimental results of the v_a and v_b phase-to-neutral grid voltages in p.u. under THD_v=5% and Unb_v=25%. Fig. 16 presents the *sine* and *cosine* for this case, where, is possible to see that the synchronism signals do not present significant distortion.

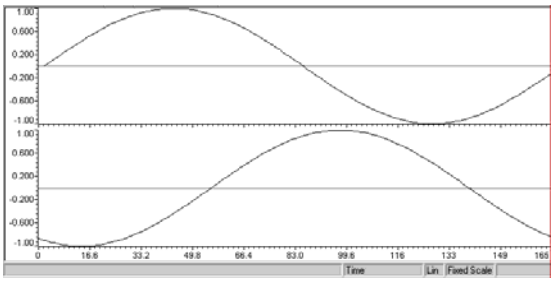

Fig. 9 – Phase-to-neutral grid voltages under THD_v=0 % and Unb_v=0%. Horizontal scale: sampling period. Vertical scale: v_a and v_b in p.u.

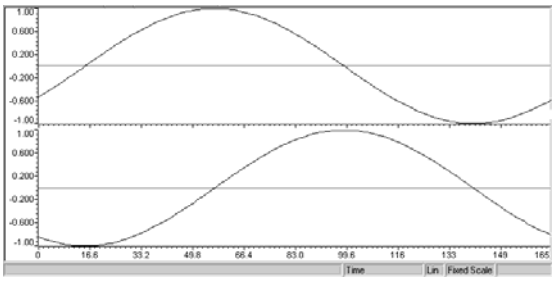

Fig. 10 – Synchronism signals obtained using the *NPSF* method under THD_v=0% and Unb_v=0% of the grid voltages. Horizontal scale: sampling period. Vertical scale: *sine* and *cosine*

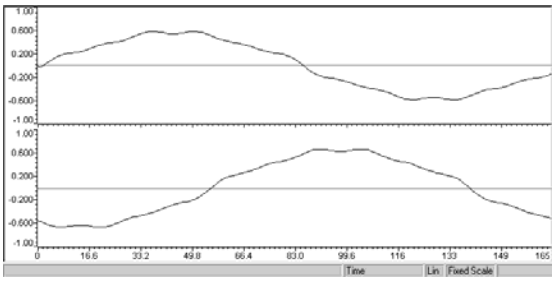

Fig. 11 – Phase-to-neutral grid voltages under THD_v=5 % and Unb_v=25%. Horizontal scale: sampling period. Vertical scale: v_a and v_b in p.u .

Fig. 12 shows the startup transient behavior of the synchronism signals of the *NPSF* method. It is possible to see a fast transient response, reaching the steady state in less than one cycle.

Fig. 13a shows the transient behavior of the control action of the frequency adaptation algorithm. A frequency step is applied in the grid voltages (58 Hz to 62.5 Hz) at time equal to 0.25 seconds. The settling time is shorter than 1.6 cycles. Fig. 13b presents the displacement power factor of the PWM converters during this transient where it is seen that it quickly recovers to a value close to 1 after the frequency transient. It is possible to see as well as a limit cycle in the estimated frequency. This is a result of the discrete number of $\boldsymbol{\Theta}$ which has been stored in the DSP program memory. However, this is not a concern, since it has a high frequency, and it can be easily mitigated with an interpolation.

Fig. 13c shows the smooth behavior of the *sine* function during the frequency transient.

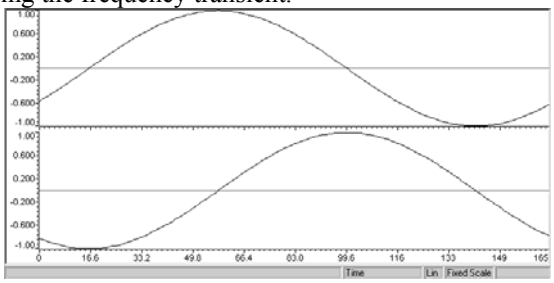

Fig. 12 – Synchronism signals obtained using the *NPSF* method under THD_v=5 % and Unb_v=25% of the grid voltages. Horizontal scale: sampling period. Vertical scale: *sine* and *cosine*.

6. Conclusion

In this paper a new synchronization method to PWM converters connected to the utility is proposed. It presents a better performance in terms of synchronism signals, if compared with other *open-loop* methods in the presence of grid voltage unbalance and harmonics, according to Table I. In addition, a frequency adaptation algorithm for applications where large frequency variations are expected, such as in weak grids, is developed.

Experimental results of the synchronism signals under unbalanced and harmonics and applied a step frequency in the grid voltages confirm the good performance of the proposed method and the frequency adaptation algorithm used in a DSP TMS320F2812.

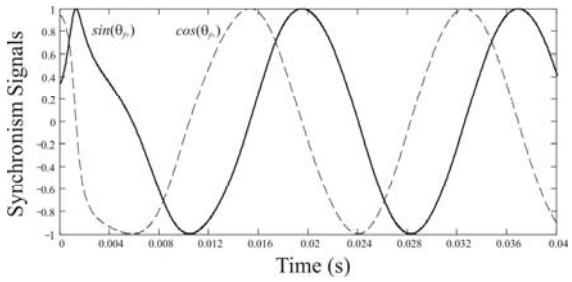

Fig. 13 – Transient behavior of the synchronism signals used the *NPSF* method.

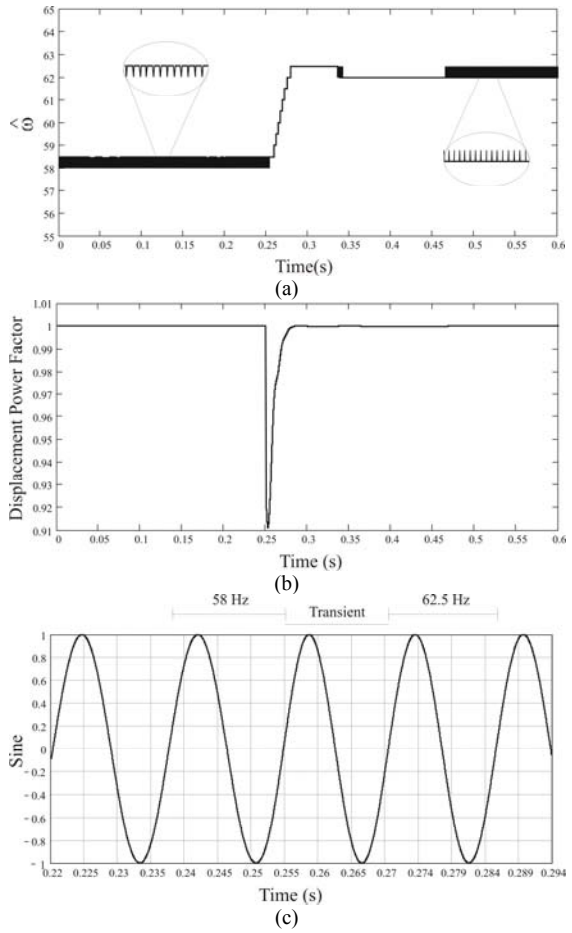

Fig. 14 – *NPSF* method used the frequency adaptation algorithm under frequency step (58Hz to 62.5 Hz). (a) Control action, (b) Displacement power factor and (c) Behavior of *sine* synchronization signal.

7. Acknowledgements

The authors would like to thank the Mr. Alexandre T. Pereira, Mr. Jorge Massing, and Mr. Felipe Grigoletto for assistance, and the CEEE, CAPES, CNPq and FAPERGS for the financial support.

.

TABLE I – OPEN-LOOP SYNCHRONIZATION METHODS WITH GRID VOLTAGE MEASUREMENT AND PERFORMANCE CRITERIA

CRITERIA / Methods	HARMONIC REJECTION	UNBALANCED REJECTION	ADAPTABILITY TO THE FREQUENCY VARIATIONS	STRUCTURAL SIMPLICITY
MSRF [6, 7]	-	-	NOT REQUIRED	HIGH
LPF-B [9]	YES	-	-	MIDDLE
SVF [9]	YES	-	-	MIDDLE
MSVF [9]	YES	-	YES	MIDDLE
EKF [9]	YES	-	YES	LOW
WLSE [15]	-	YES	YES	LOW
NPSF *	**YES**	**YES**	**YES**	**MIDDLE**

** Proposed Method*

References:

[1] G.-C. Hsieh and J. C. Hung, "Phase-locked loop techniques – A survey," *IEEE Trans. on Industrial Electronics*, vol. 43, Dec. 1996, pp. 609-615.

[2] S.-J. Lee, J.-K. Kang and S.-K. Sul, "A new phase detecting method for power conversion systems considering distorted conditions in power system," *in Proc. IAS '99*, 1999, pp. 2167 – 2172.

[3] D. R. Costa Jr., L.G.B. Rolim and M. Aredes, "Analysis and software implementation of a robust synchronizing circuit PLL circuit," *in Proc. ISIE '03*, 2003, pp. 292 – 297.

[4] S. M. Deckmann, F. P. Marafão and M. S. de Pádua, "Single and three-phase digital PLL structures based on instantaneous power theory," *in Proc. COBEP'03*, 2003, Brazil, pp. 225-230.

[5] M. Karimi-Ghartemani and M. R. Iravani, "A method for synchronization of power electronic converters in polluted and variable-frequency environments," *IEEE Trans. on Power Systems*, vol. 19, Aug. 2004, pp. 1263-1270.

[6] V. Soares and G. D. Marques, "Active power filter control circuit based on the instantaneous active and reactive current id-iq method," *in Proc. PESC'97*, 1997, pp. 1096-1101.

[7] G. D. Marques, "A comparison of active power filter control methods in unbalanced and non-sinusoidal conditions," *in Proc. IECON'98*, 1998, pp. 444-449.

[8] J. L. Duarte, A. V. Zwam, C. Wijnands and A. Vandenput, "Reference frames fit for controlling PWM rectifiers," *IEEE Trans. on Industrial Electronics*, vol. 46, Jun. 1999, pp. 628-630.

[9] J. Svensson, "Synchronization methods for grid-connected voltage source converters," *IEE Proceedings Generation Transmission and Distribution*, vol. 148, May 2001, pp. 229-235.

[10] M. Malinowski and M. P. Kasmierkowski, "Direct power control of three-phase PWM rectifier using space vector modulation-simulation study," *in Proc. ISIE'02*, 2002, pp. 1114-1118.

[11] S. Hansen, M Malinowski, F Blaabjerg and M. P. Kazmierkowski, "Sensorless control strategies for PWM rectifier," *in Proc. APEC'00*, 2000, pp. 832-838.

[12] R. M. Kennel, M. Linke and P. Szczupak, "Sensorless control of 4-quadrant-rectifiers for voltage source inverters (VSI)," *in Proc. PESC'03*, 2003, pp. 1057-1062.

[13] P. Szczupak and R. Kennel, "Sensorless control of PWM rectifiers by distorted supply voltage," *in Proc. PESC'04*, 2004, pp. 203-206.

[14] D. P. Manjure and E. B. Makram, "Impact of unbalance on power system harmonics," *in Proc. ICHQP'02*, 2002, pp. 328-333.

[15] H.-S. Song and K. Nam, "Instantaneous phase-angle estimation algorithm under unbalanced voltage-sag conditions," *IEE Proc. Generation Transmission and Distribution*, vol. 147, Nov. 2000, pp. 409-415.

[16] L. Harnefors and H.P. Nee, "A general algorithm for speed and position estimation of AC motors," *IEEE Trans. on Industrial Electronics*, vol. 47, pp. 77–83, Feb. 2000.